ACS OMEGA

Open Access

http://pubs.acs.org/journal/acsodf

Article

Understanding Thermodynamics and Kinetics of PEDOT:PSS Using ATR-FTIR and Density Functional Theory

Devyesh Rana,* John Biswakarma, and Steven R. Lustig

Cite This: *ACS Omega* 2024, 9, 38998−39003

Read Online

ACCESS | Metrics & More | Article Recommendations | Supporting Information

ABSTRACT: This work demonstrates poly(3,4-ethylenedioxythiophene) polystyrenesulfonate (PEDOT:PSS) and divinyl sulfone (DVS) cross-linking to form insoluble and porous PEDOT:PSS-DVS hydrogels. We propose a reaction mechanism and demonstrate the kinetics of a PEDOT:PSS modification that prevents PEDOT:PSS dispersibility. PSS and DVS undergo a second-order reaction between the DVS secondary carbocations and PSS oxygen anion to form a PSS-DVS network. The kinetics, from real-time attenuated total reflectance-Fourier transform infrared spectroscopy and density functional theory, reveal a temperature-dependent rate expression with a 1.458 1/s pre-exponential factor and a 2.429 kcal/mol activation energy. Cryogelation, phase separation, and phase inversion methods induce porosity in the PEDOT:PSS-DVS hydrogels with pore sizes ranging from 12 to 121 μm. Most importantly, the porous PEDOT:PSS-DVS hydrogels do not redisperse in solution. The results provide evidence for the reaction mechanism and kinetics of porous nondispersible PEDOT:PSS-DVS hydrogels.

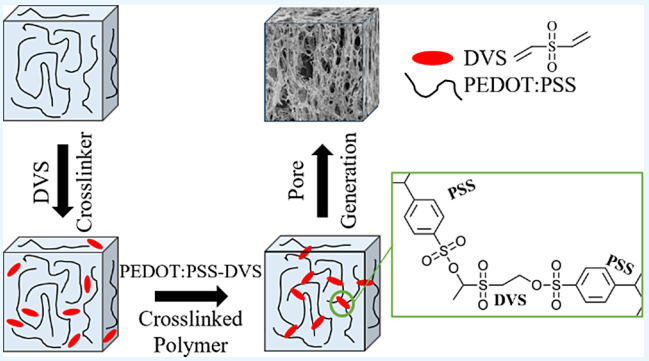

INTRODUCTION

Blends of poly(3,4-ethylenedioxythiophene) and poly(styrenesulfonate) (PEDOT:PSS) are organic conductive materials attracting a great deal of interest for use in electronics and bioengineering. PEDOT:PSS is electrically conductive, ductile, transparent, and flexible. PEDOT:PSS also easily disperses in solution, which is an advantageous property under some conditions and a disadvantage for others. A nondispersible PEDOT:PSS material can enable applications into biomaterials or electrodes to provide electrical conductivity, and porosity can support drug, or other macromolecule, delivery and fluid transport. Existing methods to prepare nondispersible and porous PEDOT:PSS hydrogels rely on mixing or in situ polymerization of PEDOT:PSS within nonconductive or conductive hydrogel templates.[1−4] Nonconductive components result in PEDOT:PSS blends with greater porosity but acts as an electrical insulator, reducing the electrical conductivity below that of pristine PEDOT:PSS. Conductive components improve the electrical conductivity compared to nonconductive components but have reduced porosity. For example, del Agua *et al.* synthesize a porous and nondispersible blend of PEDOT:PSS, xanthan gum, and DVS have 10−150 μm pores and 0.02 S cm^{-1} electrical conductivity, which is significantly less than the electrical conductivity of pristine PEDOT:PSS of 1000 S cm^{-1}.[5] Zhou *et al.* synthesize a porous and nondispersible blend of PEDOT:PSS and polyaniline that has 50 μm pores and 200 S cm^{-1} electrical conductivity using a freeze-drying process.[6] These examples demonstrate the tunability of PEDOT:PSS blends and the trade-off between porosity and electrical conductivity. Developing PEDOT:PSS blends that have greater porosity and electrical conductivity could enable improved applications in the electronic or biomaterial industries.

Nondispersible PEDOT:PSS blends cross-linked with DVS have shown increased electrical conductivity; however, limited porosity data is available. For example, del Agua *et al.* synthesized a nondispersible electrode of PEDOT:PSS, 4-dodecylbenzenesulfonic acid (DBSA), and divinyl sulfone (DVS) reacted with ethylene glycol with 605.9 S cm^{-1} electrical conductivity.[7] Mantione *et al.* synthesize nondispersible organic electrochemical transistors of PEDOT:PSS encapsulated with ethylene glycol cross-linked by DVS.[8] The electrical conductivity ranged between 550 and 750 S cm^{-1}. Sordini *et al.* use the Mantione *et al.* material for treating neurodegenerative diseases.[9] The materials made by Sordini *et al.* had 17 S cm^{-1} electrical conductivity. In all of these examples, the researchers identify that DVS-glycol cross-linking plays a crucial role in increasing the electrical conductivity and

Received: June 13, 2024
Revised: August 3, 2024
Accepted: August 23, 2024
Published: August 30, 2024

preventing the dispersion of PEDOT:PSS in solution. However, ethylene glycol is a nonconductive component that may act as an electrical insulator, and no work investigates possible direct reactions between PEDOT:PSS and DVS. Understanding the thermodynamics and kinetics between PEDOT:PSS and DVS may enable the design of new nondispersible, porous, and conductive materials.

This work explores the reaction pathway and kinetics of direct PEDOT:PSS-DVS cross-linking and synthesizes new porous PEDOT:PSS-DVS hydrogels. We consider three possible reactions for DVS protonation to which the PSS acid group can react. The reaction between PSS and DVS in the PEDOT:PSS-DVS reaction undergoes a second-order reaction for all three potential pathways. In the most favorable reaction pathway, DVS undergoes protonation to form a DVS carbonation, followed by PSS-DVS cross-linking. Finally, we demonstrate the feasibility of synthesizing nondispersible and porous PEDOT:PSS-DVS hydrogels.

MATERIALS AND METHODS

All materials were purchased and used without further purification. Dry PEDOT:PSS pellets, camphene, γ-butyrolactone, and Triton-X are purchased from Sigma-Aldrich. DVS with 0.05% hydroquinone stabilizer is purchased from Alfa Aesar.

The PEDOT:PSS-DVS hydrogels are synthesized using a PEDOT:PSS stock solution and the as-purchased DVS. An amber glass vial with the PEDOT:PSS stock solution consisted of 300 mg of PEDOT:PSS pellets dissolved in 10 mL of deionized water. A 100 μL Eppendorf tube of a PEDOT:PSS-DVS precursor contained 97 μL of the PEDOT:PSS stock solution and 3 μL of DVS. The PEDOT:PSS-DVS solution was vortexed for 5 s, pipetted onto a 10 × 10 × 1 mm^3 Teflon mold, and placed in a dark temperature-controlled enclosure for polymerization.

Porous PEDOT:PSS-DVS polymers used cryogelation, phase inversion, and phase separation for pore generation. First, we mixed the PEDOT:PSS solution (97 μL) and DVS (3 μL) at room temperature in a 1 mL Eppendorf tube. The PEDOT:PSS-DVS solution is vortexed for 5s and pipetted onto a 10 × 10 × 1 mm^3 Teflon mold. The Teflon mold is placed into a freezer at −10 °C for polymerization.[10,11] Once the polymerization is complete, the Teflon mold is placed into a vacuum chamber to remove all moisture. The remaining scaffold is the cryogelated porous PEDOT:PSS-DVS hydrogels. Porous PEDOT:PSS-DVS hydrogels made using the phase inversion technique are synthesized by first dispersing PEDOT:PSS pellets into liquid camphene at 55 °C using a hot plate and stirred until fully homogeneous to achieve a 3 w/v % PEDOT:PSS solution.[10] The mixture is kept sealed to prevent camphene evaporation. Once fully mixed, the mixture is cooled to room temperature. When ready to use, the solid camphene-PEDOT:PSS mixture is brought to 55 °C. DVS is mixed with the camphene-PEDOT:PSS solution to make 3 v/v % DVS and reacted under vacuum or in a chemical fume hood until all of the camphene has evaporated. The resulting polymer is a porous PEDOT:PSS-DVS hydrogel. Porous PEDOT:PSS-DVS hydrogels made using the phase separation technique are synthesized by first dispersing PEDOT:PSS, acetone (solvent), and Triton-X to make a 3 wt/v % PEDOT:PSS solution.[10] A 3 vol % DVS is added to the acetone-PEDOT:PSS-Triton X solution. The solution is reacted overnight in a chemical fume hood or until all of the solvent has evaporated. The hydrogel is further washed in water up to 3 times to remove Triton-X and leave behind a porous PEDOT:PSS-DVS hydrogel.

PEDOT:PSS-DVS hydrogel pore connectivity, swelling ratio, and pore size are measured. Pore size is measured by scanning electron microscopy. Dried hydrogels (10 × 10 × 1 mm^3) were mounted on the sample holder using carbon tape and sputter-coated with platinum/palladium up to 5 nm of thickness. Samples were then imaged using secondary electron detection on a Hitachi S-4800 scanning electron microscope (Hitachi High-Technology Corporation, Tokyo, Japan) while operating at 3 kV and 10 mA. Pore sizes and pore interconnectivity were quantified by measuring pore diameters using ImageJ. For measuring swelling ratio, hydrogels were prepared and immersed in deionized water for 24 h prior to the experiment. The equilibrated mass swelling ratio was calculated by dividing the mass of fully swollen hydrogels by the mass of vacuum-dried hydrogels.

To determine PEDOT:PSS-DVS kinetics, we collected real-time attenuated total reflectance-Fourier transform infrared (ATR-FTIR) spectra of PEDOT:PSS-DVS polymerization. We used a ThermoFisher Nicolet iS50R FTIR Spectrometer with a horizontal diamond ATR crystal and a liquid nitrogen-cooled MCT-B detector. The OMNIC spectroscopy software[12] recorded the average of four spectra at a 4 cm^{-1} resolution every 0.0625 s for 45 min in the range of 4000−400 cm^{-1}. The collected spectra featured an atmospheric suppression correction, automatic baseline correction, and a normalized scale. We used a custom reaction cell to maintain the sample temperatures and molecular composition. The reaction cell had a heating block with a cut out for sample staging, a resistive heating element, and a thermocouple. A BVV DHP4 temperature controller (Naperville, IL) maintained the temperature, and a cap sealed the mixture in a small volume over the ATR crystal, which prevented evaporative losses (see Figure S1). The background reference spectrum was the initial spectrum of an unreacted mixture of PEDOT:PSS, DVS, and water. A 97 μL PEDOT:PSS droplet was cast onto the ATR crystal. Next, we pipetted a 3 μL DVS droplet into the center of the PEDOT:PSS droplet and monitored the spectral changes with the FTIR until a solid polymer gel was formed and there were no more changes to the collected spectra. We calculated reaction kinetics at 30, 40, 50, and 60 °C. For the synthesis of porous PEDOT:PSS-DVS hydrogels using cryogelation, we extrapolated the time required for polymerization at −10 °C.

We used the two-dimensional correlation spectroscopy (2DCOS) method to increase the spectral resolution between overlapping ATR-FTIR peaks. Details of 2DCOS methods and their derivations are described in the works of Noda *et al.*[13] and implemented in the SpectraCorr software by Thermo Scientific. The PEDOT:PSS-DVS cross-linking real-time ATR-FTIR spectra are processed using the SpectraCorr software. The 2DCOS plots comprise synchronous, $\Phi(x, y)$, and asynchronous, $\Psi(x, y)$, functions illustrated in density maps as functions of wavenumber (x-axis) and wavenumber (y-axis). The red/yellow regions are positive correlation intensities, whereas the blue/cyan regions are negative correlation intensities. The synchronous map contains autopeaks along the diagonal line and cross-peaks located off the diagonal line. The synchronous autopeaks represent the extent of induced perturbation. Similar colored autopeaks or cross-peaks suggest that signal intensities change in the same direction, whereas dissimilar colored autopeaks or cross-peaks

https://doi.org/10.1021/acsomega.4c05552
ACS Omega 2024, 9, 38998−39003

suggest that signal intensities change in opposite directions. The asynchronous map contains only cross-peaks whose positive or negative signs reveal the sequential order of the spectral changes. Noda's rules outlined synchronous and asynchronous plot interpretation:[13]

1. if the synchronous cross-peak is positive (red/yellow), then the peak intensities on the *x*-axis and *y*-axis are moving in the same direction,
2. if the synchronous cross-peak is negative (blue/cyan), then the peak intensities on the *x*-axis and *y*-axis are moving in the opposite direction,
3. if the asynchronous cross-peak is positive (red/yellow), then the peak intensities on the *x*-axis occur before the respective change on the *y*-axis,
4. if the asynchronous cross-peak is negative (blue/cyan), then the peak intensities on the *x*-axis occur after the respective change on the *y*-axis,
5. if the synchronous cross-peak is negative (blue/cyan), then rules 3 and 4 are inversed.

The reference spectrum used to calculate the dynamic spectra in all 2DCOS calculations is the time-average of all spectra collected.

We calculated vibration modes of PEDOT:PSS, PSS, DVS, and PSS-DVS using density functional theory. DVS, PSS, PSS-DVS geometry optimizations, frequency, and Gibbs energy calculations are performed using the Jaguar[14] package as implemented within Schrodinger Maestro.[15] Calculated vibrational frequencies are derived from geometry-optimized ground-state molecular structures. Geometry optimizations use a 6-31G** basis set and nonlocal Perdew–Burke–Ernzerhof pure functional.[16] The self-consistent field density convergence was set to 10^{-6} Ha using energy minimized species as the initial structure guess. The calculated vibrational spectra are checked to ensure the structures are ground states. The calculated vibration modes are given in Table S1. The reaction Gibbs energies and activation energies used the reactant, intermediate, and product Gibbs energies.

RESULTS AND DISCUSSION

Thermodynamics of PEDOT:PSS-DVS Cross-Linking. We evaluated three types of PEDOT:PSS-DVS cross-links. There are three potential reaction sites for DVS protonation in an acid solution, illustrated in Figure 1. Products 1, 2, and 3 produce PSS-DVS cross-links via sulfur dioxide protonation, vinyl protonation of a secondary carbon, and vinyl protonation of a primary carbon, respectively. The calculated Gibbs energies of the reaction are −7.50, −9.02, and −8.21 kcal/mol for Products 1, 2, and 3, respectively. These results are consistent with the Markovnikov Rule[17] that predicts the regiochemistry of hydrogen addition reactions of alkenes and alkynes. Specifically, the electron-rich component of the reaction adds to the carbon atom with fewer hydrogen atoms bonded to it, while the electron-deficient component adds to the carbon atom with more hydrogen atoms bonded to it. The DVS molecule has more hydrogen atoms on the primary carbon and fewer hydrogen atoms on the secondary carbon. Therefore, based on the Markovnikov rule, it is likely that the electron-rich PSS molecule would react with the DVS carbon with fewer hydrogen atoms bonded to it. Finally, we find that the reaction mechanisms followed a second-order effective rate law dependent on the concentration of DVS, shown in eqs 1 and 2. We hypothesize that Product 2 is the most likely

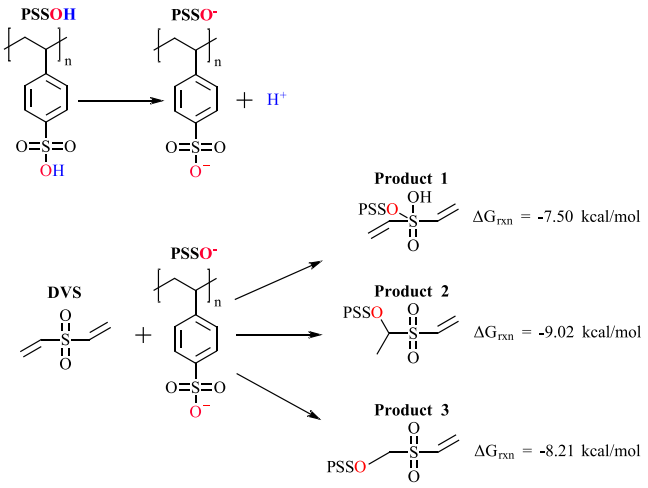

Figure 1. Three potential PSS-DVS reaction mechanisms and associated calculated Gibbs energies of the reaction.

reaction pathway based on the Gibbs energies of reaction and the Markovnikov Rule.

$$\mathrm{DVS} + \mathrm{PSSH} \rightarrow \mathrm{PSS} - \mathrm{DVS} \tag{1}$$

$$r_{\mathrm{PSSDVS}} = -\frac{\mathrm{d[DVS][PSSH]}}{\mathrm{d}t} = k[\mathrm{DVS}][\mathrm{PSSH}] \tag{2}$$

There are other PEDOT:PSS-DVS cross-linking sites; however, they are unlikely to occur. We find that binding of DVS to the PSS benzene ring or the PSS backbone is not exergonic, as shown in Figure S2. This finding is consistent for cross-links via the DVS sulfur dioxide protonation, vinyl protonation of the secondary carbon, and vinyl protonation of the primary carbon.

Kinetics of PEDOT:PSS-DVS Cross-Linking. The temporal order of chemical changes that occur during the cross-linking process is resolved by applying 2DCOS to time-resolved ATR-FTIR spectra of the PEDOT:PSS-DVS reaction. The synchronous, Φ, and asynchronous, Ψ, correlation intensities are obtained from the time-resolved ATR-FTIR spectra ranging in time from initial DVS addition to reaction completion; see Figure 2. The peak locations and sequential changes indicated by 2DCOS are listed in Table S1. In the synchronous correlation map, seven major auto peaks are observed at 985, 1130, 1300, 1335, 1390, 1540, and 1650 cm^{-1}. The cross-peaks are considered in two groups. Group A includes 985, 1130, 1300, and 1390 cm^{-1}; group B includes 1135, 1540, and 1650 cm^{-1}. Group A wavenumbers

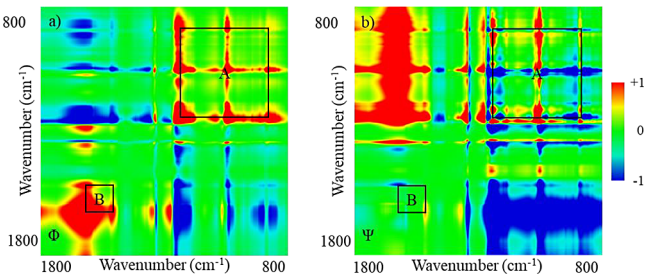

Figure 2. Representative (a) synchronous Φ and (b) asynchronous correlations Ψ of PEDOT:PSS-DVS spectra at 25 °C. Color indicates peak sign: red/yellow is positive, green is near zero, and blue/cyan is negative.

https://doi.org/10.1021/acsomega.4c05552
ACS Omega 2024, 9, 38998−39003

correspond to the carbon−carbon double bond of DVS, whereas group B wavenumbers correspond to the oxygen−carbon bond between PSS and DVS. The synchronous correlation map, Figure 2a, consists of numerous independent cross-peaks. Group A cross-peaks are positive in sign, indicating that group A intensities simultaneously change. Group B cross-peaks are positive in sign, indicating that group B intensities also simultaneously change together. However, since the cross-peaks between groups A and B are opposite in sign, group A intensities change separately from group B intensities. The asynchronous correlation map, Figure 2b, directly provides the order of events. The relationship between groups A and B may provide the order for PEDOT:PSS-DVS polymerization. The asynchronous cross-peak between groups A and B is positive, indicating that group A bands decrease first, followed by an increase in group B bands.

Analysis of time-resolved FTIR data provides strong evidence for PSS-DVS bonding via DVS vinyl protonation on either the primary or secondary carbons. We first note that the calculated and ATR-FTIR measured vibration modes agree for DVS and PEDOT:PSS raw materials, as shown in Figure S3. Calculated product 1, 2, and 3 vibration modes, summarized in Table S2, correspond to the auto peaks from 2DCOS results. Group A vibration modes, from Figure 3,

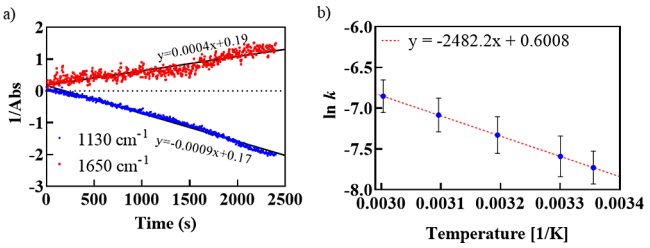

Figure 3. Representative absorbance vs time charts (left). An Arrhenius plot for the second-order kinetics of vinyl degradation using rate constants for different temperatures (right). The error bars indicate the standard deviation in rate constants resulting from multiple experiments (n = 3).

correspond to the carbon−carbon double bond on the DVS molecule. Group B vibration modes from Figure 3 correspond to PSS-DVS product formation. The carbocation intermediate to Product 3 may undergo a hydride shift and rearrange into Product 2 due to the greater stability of secondary carbon carbocations over primary carbon carbocations, as suggested by the lower Gibbs energy of Product 2 than Product 3. However, the similar vibration frequencies of Products 2 and 3 suggest that one or both may be present and that they could form major and minor products, respectively, following the Markovnikov Rule.[17] We also rule out the formation of Product 1 due to the nonoxidizing nature of sulfones, as described by the Ramberg-Backlund reaction and Julia olefination.[18,19] This is also supported by the lack of matching of calculated and ATR-FTIR vibrational modes for sulfur dioxide protonation. Both Products 2 and 3 have similar vibrational modes, as shown in Table S2, making it difficult to distinguish between the two products. This also makes it difficult to identify which product may be more beneficial for biomaterial or electronic applications and could be of interest for future studies. It may be possible to select which product forms by increasing the vinyl chain or by adding halogen substituents.[20]

Time-resolved ATR-FTIR spectra reveal the rate of change in the peak intensity for specific vibrational modes. The results in Figure 3a show that the reactions that occur in a 3 wt/v % PEDOT:PSS and 3 v/v % DVS solution complete within 40 min at room temperature. The area of the absorbance peaks at 1130 and 1650 cm^{-1} corresponding to DVS vinyl degradation and PSS-DVS reaction, respectively, is monitored over time. The rate constants, Figure 3b, are calculated at varying temperatures between 25 and 60 °C. Temperature-dependent rate laws are determined by obtaining the pre-exponential factor and activation energy from the rate constant versus temperature plots using a natural logarithmic fit. The Arrhenius rate expression describing PSS-DVS cross-linking derived from the time-resolved absorbance at 1130 cm^{-1} is shown as eq 3 with a 1.458 1/s pre-exponential factor and a 2.429 kcal/mol activation energy. The pre-exponential factor is associated with the frequency of collisions between molecules, with reaction entropy, and with the probability that these collisions result in a reaction. The pre-exponential factor and activation energy tell us that the reaction from reactants to the intermediates is a slow process; however, the reaction from intermediates to the final product will be fast. The kinetics data provide evidence that the area over time graphs resemble a second-order reaction, confirming eqs 1 and 2 for the overall mechanism and governing equations of PEDOT:PSS-DVS formation.

$$k = 1.458\exp\left(\frac{2.429\ \frac{\text{kcal}}{\text{mol}}}{RT}\right)\text{mol}^{-1}\text{s}^{-1} \quad (3)$$

The calculated and experimental activation energies provide evidence of the product 2 formation. The activation energies for products 1, 2, and 3, shown in Figure 4, are 6.59, 2.44, and

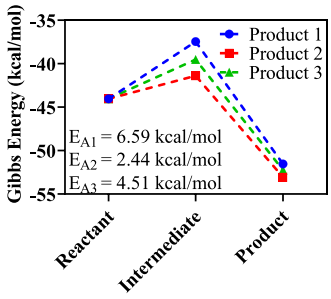

Figure 4. Gibbs energies of reactants, intermediates, and products corresponding to reactions 1−3. The Gibbs energies of the reactant and product species correspond to the molecules shown in Figure 1. The Gibbs energies reported for intermediate species are the sum of Gibbs energies of the DVS carbocation and PSS anion. The activation energies for each reaction pathway are listed in the inset.

4.51 kcal mol^{-1}, respectively. The calculated activation energy for product 2 is the lowest among those of the reaction pathways considered. Therefore, protonation of the secondary carbon is more energetically favorable than protonation of the DVS sulfur atom and primary carbon. The calculated activation energy of product 2 differs from the experimental activation energy (2.429 kcal mol^{-1}) by less than 1%. The similarity between calculated and experimental activation energies once again gives us confidence that product 2 is the likely reaction pathway product.

https://doi.org/10.1021/acsomega.4c05552
ACS Omega 2024, 9, 38998−39003

Finally, we apply our understanding of the reaction mechanism and kinetics to fabricate nondispersible porous PEDOT:PSS-DVS hydrogels using pore-inducing techniques. Pore generation enables fluid transport or drug delivery depending on the application, which makes porosity and pore size tunability important. Here, we employ cryogelation, phase inversion, and phase separation to create a tunable porosity in our PEDOT:PSS hydrogels. Figure 5 shows the pore size, pore

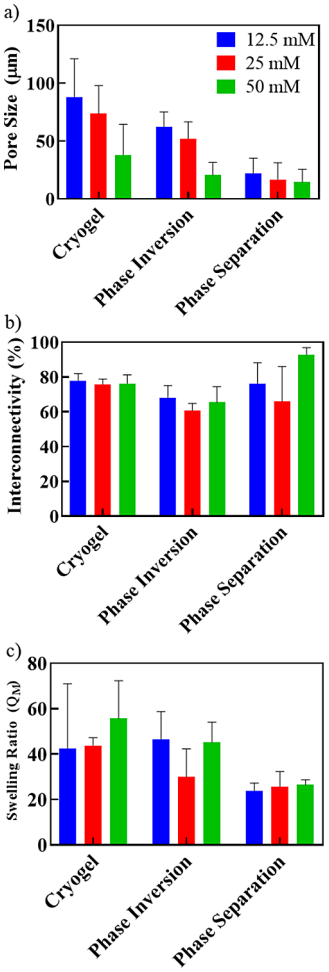

Figure 5. Average (a) pore size, (b) pore interconnectivity, and (c) swelling ratio of PEDOT:PSS-DVS hydrogels fabricated using cryogelation, phase inversion, and phase separation with 12.5, 25, and 50 mM PEDOT:PSS and 3 v/v % DVS.

interconnectivity, and swelling ratio measurements. Hydrogels consist of a three-dimensional network of interconnected macropores[11] (pores $\geq$ 10 μm). Cryogelated PEDOT:PSS-DVS hydrogels have higher pore sizes compared to those of their phase-inverted and phase-separated counterparts. For example, pore sizes of cryogelated, Figure 6a, phase inverted, Figure 6b, and phase separated, Figure 6c, PEDOT:PSS-DVS hydrogels with 12.5 μM of PEDOT:PSS are 88 $\pm$ 33, 73 $\pm$ 24, and 38 $\pm$ 26 μm, respectively. Increasing polymer concentration from 12.5 to 25 to 50 μM decreases the pore sizes for all polymer combinations, as shown in Figure 5a. The PEDOT:PSS blend hydrogels produced here are 81 and 41% of previously reported PEDOT:PSS blends.[5,6] Figure 6 shows hydrogel interconnectivity, and Figure 5b shows the associated SEM images. Cryogelated, phase-inverted, and phase-separated

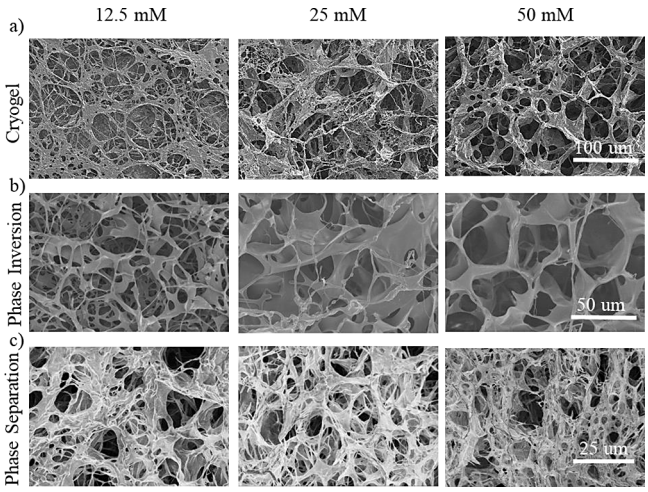

Figure 6. Representative SEM graphs of porous PEDOT:PSS-DVS hydrogels fabricated using (a) cryogelation, (b) phase inversion, and (c) phase separation prepared with 12.5, 25, and 50 mM PEDOT:PSS and 3 v/v % DVS.

PEDOT:PSS-DVS hydrogels all have greater than 60% interconnectivity. The swelling ratio of all hydrogels decreases the water retention as polymer concentration increases, as shown in Figure 5c, which is a typical observation given a consistent volume of hydrogel. Most importantly, porous PEDOT:PSS-DVS hydrogels do not disperse in solution after fabrication. In conclusion, we demonstrate the ability to manipulate the reaction kinetics, such as in the case of cryogelation, to fabricate porous PEDOT:PSS-DVS hydrogels that do not disperse in solution.

CONCLUSIONS

PEDOT:PSS application range has been limited due to its dispersibility in solution. Here, we develop nondispersible and porous PEDOT:PSS-DVS hydrogels. We propose a reaction mechanism and investigate the kinetics for PEDOT:PSS-DVS hydrogel synthesis using RT-ATR-FTIR. Vibrational modes of PEDOT:PSS, DVS, and PEDOT:PSS-DVS are identified using quantum mechanical calculations and ATR-FTIR. We also propose an Arrhenius expression for the temperature-dependent reaction rate for PEDOT:PSS-DVS formation. Finally, we fabricate porous PEDOT:PSS-DVS hydrogels by using cryogelation, phase inversion, and phase separation. These fabricated hydrogels and demonstrated chemistry show that PEDOT:PSS is cross-linkable, enabling new avenues for PEDOT:PSS applications.

ASSOCIATED CONTENT

Supporting Information

The Supporting Information is available free of charge at https://pubs.acs.org/doi/10.1021/acsomega.4c05552.

Experimental apparatus; additional investigated reactions; comparison of calculated and experimental vibrational wavenumbers; sequential order of vibrational modes; and full table of all vibrational wavenumbers (PDF)

https://doi.org/10.1021/acsomega.4c05552
ACS Omega 2024, 9, 38998−39003

AUTHOR INFORMATION

Corresponding Author

Devyesh Rana − *Department of Chemical Engineering, Northeastern University, Boston, Massachusetts 02115, United States;* orcid.org/0000-0003-3961-6227; Email: rana.de@northeastern.edu

Authors

John Biswakarma − *Department of Chemical Engineering, Northeastern University, Boston, Massachusetts 02115, United States*

Steven R. Lustig − *Department of Chemical Engineering, Northeastern University, Boston, Massachusetts 02115, United States;* orcid.org/0000-0001-5030-852X

Complete contact information is available at: https://pubs.acs.org/10.1021/acsomega.4c05552

Author Contributions

D.R.: conceptualization, experimental design, performed experiments, data analysis, and writing. J.B.: 2DCOS spectroscopy, reviewing and editing. S.R.L.: conceptualization, software design and composition, training, experimental design, writing, reviewing, editing. All authors have approved of the final version of the manuscript.

Notes

The authors declare no competing financial interest.

ACKNOWLEDGMENTS

SRL's access to Materials Studio and DMol3 is made possible by the BIOVIA Science Ambassador Program.

REFERENCES

(1) Feig, V. R.; Tran, H.; Lee, M.; Bao, Z. Mechanically tunable conductive interpenetrating network hydrogels that mimic the elastic moduli of biological tissue. *Nat. Commun.* **2018**, *9* (1), 2740.

(2) Lee, Y.-Y.; Kang, H.-Y.; Gwon, S. H.; Choi, G. M.; Lim, S.-M.; Sun, J.-Y.; Joo, Y.-C. A Strain-Insensitive Stretchable Electronic Conductor: PEDOT:PSS/Acrylamide Organogels. *Adv. Mater.* **2016**, *28* (8), 1636−1643.

(3) Warren, H.; Panhuis, M. Electrically Conducting PEDOT:PSS − Gellan Gum Hydrogels. *MRS Online Proceedings Library* **2013**, *1569* (1), 219−223.

(4) Goding, J.; Gilmour, A.; Martens, P.; Poole-Warren, L.; Green, R. Interpenetrating Conducting Hydrogel Materials for Neural Interfacing Electrodes. *Adv. Healthcare Mater.* **2017**, *6* (9), No. 1601177.

(5) del Agua, I.; Marina, S.; Pitsalidis, C.; Mantione, D.; Ferro, M.; Iandolo, D.; Sanchez-Sanchez, A.; Malliaras, G. G.; Owens, R. M.; Mecerreyes, D. Conducting Polymer Scaffolds Based on Poly(3,4-ethylenedioxythiophene) and Xanthan Gum for Live-Cell Monitoring. *ACS Omega* **2018**, *3* (7), 7424−7431.

(6) Zhou, Q.; Teng, W.; Jin, Y.; Sun, L.; Hu, P.; Li, H.; Wang, L.; Wang, J. Highly-conductive PEDOT:PSS hydrogel framework based hybrid fiber with high volumetric capacitance and excellent rate capability. *Electrochim. Acta* **2020**, *334*, No. 135530.

(7) del Agua, I.; Mantione, D.; Ismailov, U.; Sanchez-Sanchez, A.; Aramburu, N.; Malliaras, G. G.; Mecerreyes, D.; Ismailova, E. DVS-Crosslinked PEDOT:PSS Free-Standing and Textile Electrodes toward Wearable Health Monitoring. *Adv. Mater. Technol.* **2018**, *3* (10), No. 1700322.

(8) Mantione, D.; del Agua, I.; Schaafsma, W.; ElMahmoudy, M.; Uguz, I.; Sanchez-Sanchez, A.; Sardon, H.; Castro, B.; Malliaras, G. G.; Mecerreyes, D. Low-Temperature Cross-Linking of PEDOT:PSS Films Using Divinylsulfone. *ACS Appl. Mater. Interfaces* **2017**, *9* (21), 18254−18262.

(9) Sordini, L.; Garrudo, F. F. F.; Rodrigues, C. A. V.; Linhardt, R. J.; Cabral, J. M. S.; Ferreira, F. C.; Morgado, J. Effect of Electrical Stimulation Conditions on Neural Stem Cells Differentiation on Cross-Linked PEDOT:PSS Films. *Front. Bioeng. Biotechnol.* **2021**, *9*, No. 591838.

(10) Lustig, S.; Rana, D.; Lachmayr, K. Engineering a porous conductive PEDOT:PSS-DVS scaffold for microbial fuel cell air cathodes. 20210324169, 2021.

(11) Rana, D.; Colombani, T.; Saleh, B.; Mohammed, H. S.; Annabi, N.; Bencherif, S. A. Engineering injectable, biocompatible, and highly elastic bioadhesive cryogels. *Materials Today Bio* **2023**, *19*, No. 100572.

(12) T. F. S. Inc. *OMNIC 9, 9.8.372*; 2017.

(13) Noda, I. Generalized Two-Dimensional Correlation Method Applicable to Infrared, Raman, and Other Types of Spectroscopy. *Appl. Spectrosc.* **1993**, *47* (9), 1329−1336.

(14) Bochevarov, A. D.; Harder, E.; Hughes, T. F.; Greenwood, J. R.; Braden, D. A.; Philipp, D. M.; Rinaldo, D.; Halls, M. D.; Zhang, J.; Friesner, R. A. Jaguar: A high-performance quantum chemistry software program with strengths in life and materials sciences. *Int. J. Quantum Chem.* **2013**, *113* (18), 2110−2142.

(15) Schrodinger, L. *Maestro 2020-4*; New York, NY.

(16) Perdew, J. P.; Burke, K.; Ernzerhof, M. Generalized Gradient Approximation Made Simple. *Phys. Rev. Lett.* **1996**, *77* (18), 3865−3868.

(17) Beletskaya, I. P.; Nenajdenko, V. G. *Towards the 150th Anniversary of the Markovnikov Rule.* **2019**, *58* (15), 4778−4789.

(18) Taylor, R. J. K. Recent developments in Ramberg−Bäcklund and episulfone chemistry. *Chem. Commun.* **1999**, *3*, 217−227.

(19) Julia, M.; Paris, J.-M. Syntheses a l'aide de sulfones v(+)-methode de synthese generale de doubles liaisons. *Tetrahedron Lett.* **1973**, *14* (49), 4833−4836.

(20) Vrček, V.; Vrček, I. V.; Kronja, O. Mechanism of 1,2-Hydride Shift in Some Carbocations Involved in Steroid Biosynthesis. *Croat. Chem. Acta* **2001**, *74* (4), 801−813.

https://doi.org/10.1021/acsomega.4c05552
ACS Omega 2024, 9, 38998−39003